# FLOW VISUALIZATION AND PIV MEASUREMENTS OF LAMINAR SEPARATION BUBBLE OSCILLATING AT LOW FREQUENCY ON AN AIRFOIL NEAR STALL

**Hiroyuki Tanaka**
**Department of Aeronautics & Astronautics**
**University of Tokyo, 113-8656, Japan**

**Keywords**: *laminar separation bubble, stall, low-frequency oscillation, PIV, wavelet analysis*

## Abstract

*Laminar separation bubbles formed on a NACA 0012 airfoil were investigated to clarify the mechanism of their quasi-periodic behaviors near the onset of airfoil stall (angles of attack around $\alpha = 11.5°$). The Reynolds number based on the airfoil chord was $Re_c = 1.3\times10^5$.*

*Smoke flow visualization images showed that the flow over the airfoil is oscillating at a low frequency near stall. This oscillation is a switching between a flow that is attached to the airfoil surface and a flow that is largely separated from the surface. Flow velocity near the leading edge fluctuated in synchronization with this flow oscillation. Wavelet analysis was applied to this velocity fluctuation at some different angles of attack near stall. The results revealed that the frequency of the flow oscillation increases as the angle of attack is increased within the range of angles of attack near stall. Instantaneous flowfield was investigated by particle image velocimetry. The results indicated that a separation bubble is formed when the flow is attached to the surface. Large vortices that change the flowfield over the airfoil were observed when the flow switches from a large separated state to an attached flow.*

## Nomenclature

| | |
|---|---|
| $c$ | airfoil chord length, m |
| $C_p$ | pressure coefficient based on free stream static and dynamic pressures |
| $f$ | frequency of flow oscillation, Hz |
| $Re_c$ | Reynolds number based on the airfoil chord length |
| $St$ | Strauhal number = $fc\sin\alpha/U_\infty$ |
| $U$ | component of instantaneous velocity along $x$-axis, m/s |
| $U_\infty$ | free stream velocity, m/s |
| $V$ | component of instantaneous velocity along $y$-axis, m/s |
| $x$ | Cartesian coordinate along the free stream direction measured from the leading-edge of the airfoil, m |
| $x_c$ | coordinate along the airfoil chordline measured from the leading-edge, m |
| $y$ | Cartesian coordinate perpendicular to $x$ and measured from the leading edge, m |
| $\alpha$ | airfoil angle of attack, degree |
| $\phi$ | phase angle, degree |
| $\omega$ | spanwise vorticity, 1/sec |

## 1 Introduction

In a flow around an airfoil, when a laminar boundary layer separates from the airfoil surface, the flow often attaches to the surface some distance downstream as a turbulent boundary layer. This separated region between laminar separation and reattachment is referred to as a laminar separation bubble. A laminar separation bubble formed on an airfoil is classified into two types: a short bubble and a long bubble [1]. A short bubble is formed when the airfoil angle of attack is relatively small. As the angle of attack is increased, the short bubble abruptly fails to reattach to the airfoil surface. This phenomenon is known as the short bubble burst. When the separated layer extends toward the airfoil wake and the whole upper surface is covered by this large separated flow, the lift of

the airfoil decreases sharply (a leading-edge stall). On the other hand, when the separated shear layer reattaches to the surface once again, a long bubble is formed. A negative pressure peak near the leading edge in a short bubble is lost, and the surface pressure distribution in a long bubble indicates a relatively flattened form. In this way, laminar separation bubbles on an airfoil highly influence the stall characteristics of the airfoil.

Low-frequency flow oscillations have been observed in laminar separation bubbles. Hata et al. [2] reported a fluctuation at about 100 Hz in a short bubble formed on a NACA 0012 airfoil ($Re_c = 1.3\times10^5$, $\alpha = 10°$).

It has been suggested that the flow around an airfoil near stall is highly unsteady and oscillating flow. Unsteady flow oscillations at much lower frequencies have been reported on airfoils at angles of attack near stall [3]-[8]. Zaman et al. [3] conducted computational and experimental studies on this type of flow oscillation that occurs on an LRN(1)-1007 airfoil at a low Reynolds number ($Re_c = 1.3\times10^5$, $\alpha \approx 11.5°$). The authors reported that the oscillation was a quasi-periodical switching between stalled and unstalled conditions. They also concluded that the origin of the flow fluctuation traces to the upper surface of the airfoil near the leading edge, and the fluctuation decays rapidly downstream. The Strauhal number of the oscillation observed in this study was $St \approx 0.02$. Ref. 3 also concluded that this oscillation was not due to any peculiarity of the facility and was fluid dynamic by nature.

Bragg et al. [4] observed a similar flow oscillation of $St \approx 0.005$. These $St$'s are much lower than that observed in an oscillating wake of a bluff body ($St \approx 0.2$). Further researches [5]-[7] discussed that a laminar separation bubble is formed when in an unstalled condition. Ref. 7 also performed thorough wind tunnel tests of various airfoils and reported that this flow oscillation occurs only on airfoils that exhibit the stall characteristics of thin-airfoil stall or the combination of thin-airfoil stall and trailing-edge stall.

Rinoie et al. [8] conducted flowfield measurements in order to investigate the low-frequency oscillation on a NACA 0012 airfoil near stall. Flow visualization pictures indicated a low-frequency oscillation of $St \approx 0.008$ (2 Hz) at the angle of attack near the onset of stall ($Re_c = 1.3\times10^5$, $\alpha = 11.5°$). In Ref. 8, phase averaged velocity measurements were performed. The results are shown in Fig. 1. Fig.1 (a) shows the velocity fluctuation near the leading edge, which was used as the reference signal in the phase averaging technique. This velocity will be referred to as the 'reference velocity.' The phase was defined based on the peaks of the reference signal. Fig. 1 (b) shows the phase averaged velocity distributions measured by two-dimensional laser Doppler anemometry (2D-LDA). At $\phi = 0°$, a small separation-reattachment bubble of about 10 % chord length is formed near the leading edge. At $\phi = 180°$, a large separated region extends over the airfoil. The flow over the airfoil is switching between these two states. The authors discussed that the small separation-reattachment bubble has relatively similar flow structures to that of a short bubble formed at a lower angle of attack ($\alpha = 10°$) by comparing the phase averaged velocity distributions and the turbulent normal stress distributions (Fig. 1 (c)).

From the results of the same experiment as Ref. 8, Takemura et al. [9] conducted phase averaged turbulent energy balance analyses. The authors suggested that the increase in turbulent stress based on turbulent energy production and the diffusion effect of turbulent flow lead to the formation of the large separated region.

Ref. 10 investigated the low-frequency flow oscillation qualitatively by means of flow visualization using the same airfoil model as Refs. 2, 8 and 9. It was reported that the quasi-periodic oscillation of 2 Hz exists only at $\alpha = 11.5°$. At a lower angle of attack ($\alpha = 11.3°$), the flow is attached to the airfoil surface for most of the time and occasionally switches to a large separated flow. At a higher angle of attack ($\alpha = 11.8°$), the flow is largely separated from the airfoil surface for most of the time and occasionally switches to an attached flow. From

these results, it was suggested that this flow oscillation is not a quasi-periodic phenomenon which occurs only at $\alpha = 11.5°$: the quasi-periodic flow oscillation at $\alpha = 11.5°$ is rather a part of unsteady flow behaviors which are not necessarily periodic phenomena and are widely present among angles of attack near stall ($\alpha$ = 11° - 12°).

However, the mechanism that causes the low-frequency oscillation of a separation bubble near stall still remains unclear. In this study, the flow oscillation observed on a NACA 0012 airfoil at angles of attack near stall that was discussed qualitatively in Ref. 10 was investigated further in detail by using more quantitative techniques. The experiments were performed at a chord Reynolds number of $Re_c = 1.3\times10^5$. Smoke flow visualizations were conducted to understand the overview of this flow oscillation. Wavelet analysis was applied to instantaneous velocity fluctuations measured near the leading edge at several angles of attack near stall. This technique was utilized in this study because it is capable of analyzing the frequencies of non-periodic oscillations, which were reported to occur at some angles of attack near stall in Ref. 10. The flow oscillations at various angles of attack are discussed quantitatively based on the results of wavelet analysis. Furthermore, the instantaneous flowfield during the flow oscillation was investigated in detail by utilizing particle image velocimetry (PIV) to supplement the smoke flow visualization results with more quantitative discussion.

## 2 Experimental Details

Measurements were performed in a low speed suck-down type wind tunnel with a test section of 0.6 m in height, 0.2 m in width and 1 m in length. The free stream turbulence intensity at the test section is less than 0.16 %. The free stream velocity was set to $U_\infty$ = 10 m/s. A NACA 0012 airfoil model of 0.2 m span was mounted in the wind tunnel. The chord length of the model is $c$ = 0.2 m. This airfoil model is the one used in Refs. 2, 8 - 10. The chord Reynolds number is $Re_c = 1.3\times10^5$.

Smoke flow visualizations were performed to understand the overview of the quasi-periodic behavior of the flow in the chordwise plane normal to the airfoil surface. Oil mist made of Ondina oil was used as flow visualization particles. A 500 W halogen lump was used as a light source (the width of the light sheet was approximately 5 mm). The visualized flow was recorded using a PHOTORON FASTCAM-Ultima-I$^2$ high-speed video camera (4500 maximum frames/sec, 256×256 pixels, equipped with an image intensifier of 160 dB maximum gain). For the present study, images were taken at a rate of 500 frames/sec, and the image resolution was 256 × 256 pixels. The acquired image data was recorded by a PC.

The velocity at a point near the leading edge, which indicates the state of the flow over the airfoil [10], was measured for the wavelet analysis. This velocity in the free stream direction was measured by a one-component laser Doppler anemometry (DANTEC 55X, 1D-LDA) in forward scattering mode. This measurement was carried out at the point where the reference velocity was measured in Refs. 8 and 9 ($x/c$ = 0.011, $y/c$ = 0.015 when the airfoil angle of attack was set to $\alpha = 11.5°$). This measurement point was fixed even when the airfoil angle of attack was changed. The Doppler signals were processed by a DANTEC 55N20 frequency tracker and a DANTEC 55N10 frequency shifter. The velocity signals from these processors were then transmitted to a PC through an A/D converter.

Instantaneous planer velocity fields were measured via PIV. A double-pulse Nd: YAG laser (50 mJ/pulse, 15 Hz) was used to illuminate the oil mist. The laser pulse duration was 0.01 μsec, and the separation of the two pulses was set to 10 μsec. The images were recorded by a 1008×1018 pixel Kodak Megaplus ES1.0 camera equipped with a Nikkor 200 mm lens. The measurements were carried out at a sampling rate of 5 Hz. The double exposed digital images by two separate pulses were then processed by a Dantec PIV2000

processor using a Fast Fourier Transform (FFT)-based autocorrelation algorithm. A 61×61 velocity vector map was obtained from this process using an interrogation area size of 32×32 pixels. It should be noted that the sampling rate of the PIV (5 Hz) is too small to track the flow oscillation under discussion (about 2 Hz). To overcome this problem, velocity measurements by the 1D-LDA, which was described previously, were performed simultaneously with the PIV measurements. To synchronize the results of these two measurements, the PIV laser pulse signals were recorded together with the 1D-LDA data.

## 3 Wavelet Analysis

Fourier analysis is most commonly used in data analyses. However, it is difficult to analyze frequencies that change with time by Fourier analysis. In order to be used in such cases, wavelet analysis was developed [11]. Wavelet analysis has been applied to fluid mechanics in recent years. There are two kinds of wavelet analyses: continuous wavelet analysis and discrete wavelet analysis. In this study, the continuous wavelet analysis, which has been commonly used in analyses in the fluid mechanics, is used.

The continuous wavelet transform of a real square integrable function $f(t) \in L^2(R)$ is defined as

$$Wf(b,a) = \frac{1}{\sqrt{a}} \int_{-\infty}^{\infty} f(t) \overline{\psi\left(\frac{t-b}{a}\right)} dt \qquad (1)$$

Here, $Wf(b, a)$ is referred to as the wavelet coefficient, and $\bar{}$ represents the complex conjugate. The parameters $b$ and $a$ correspond to the time and the scale relative to the analyzing wavelet respectively. $\psi(t)$ is called the analyzing wavelet and is required to satisfy the following condition (admissible condition).

$$C_\phi = \int_{-\infty}^{\infty} \frac{\left|\hat{\psi}(\omega)\right|^2}{|\omega|} d\omega < \infty \qquad (2)$$

Some functions such as Haar, Mexican hat, Morlet and Gabor wavelet are commonly used as the analyzing wavelet. In this study, Morlet function was chosen. This function is given by

$$\psi(t) = \pi^{-\frac{1}{4}} e^{-i\omega_0 t} e^{-\frac{t^2}{2}}, \qquad (3)$$

and its Fourier transform is written as

$$\hat{\psi}(\omega) = \sqrt{2}\pi^{\frac{1}{4}} e^{-(\omega-\omega_0)^2/2}. \qquad (4)$$

The Morlet function $\psi(t)$ is localized around $t$ = 0, and its Fourier transform $\hat{\psi}(\omega)$ is localized around the central frequency of passing band $\omega_c = \omega_0$. It is very useful to define as $\omega_c = \omega_0 = 2\pi$ so that the parameter $a$ represents the period [12]. For this reason, this value of $\omega_0 = 2\pi$ was used in this study. The real part of the wavelet coefficient $Wf(b, a)$, which is related to both the amplitude and the phase of the waveform, will be used to discuss the flow characteristics inside the laminar separation bubble.

## 4 Results and Discussions

Fig.2 shows the surface pressure ($C_p$) distributions plotted against the chordwise direction for different angles of attack [2]. This figure indicates that a short bubble is formed when the angle of attack is $\alpha = 10°$ (see a high suction pressure near the leading edge followed by a plateau and a sudden pressure recovery). The chordwise length of the short bubble is approximately 10 % of the airfoil chord. The high suction pressure near the leading edge is lost at $\alpha = 11.5°$. The sudden pressure recovery is also lost at $\alpha = 11.5°$. This indicates that the short bubble burst has occurred. At $\alpha = 12°$, the pressure distribution on the upper surface becomes flat, suggesting that the laminar separation bubble has completely shifted to a long bubble. It is also reported that the flowfield quasi-periodically oscillates at low frequency at $\alpha = 11.5°$ in Refs. 8 - 10. Ref. 10 also reported similar flow oscillations at other angles of attack near the onset of stall ($\alpha = 11° - 12°$). Therefore,

measurements were carried out at angles of attack within the range of $\alpha = 11° - 12°$.

### 4.1 Overview of the Flow Oscillation

Fig. 1 (a) shows the reference velocity fluctuation at $\alpha = 11.5°$ [8], as was already explained. The reference velocity is the velocity in the free-stream direction at a point near the leading edge. The reference velocity in Fig. 1 (a) was measured by the 1D-LDA, which was described earlier. Fig. 3 shows some examples of the smoke flow visualization images at $\alpha = 11.5°$ acquired by the high-speed video camera. The flow is from left to right. The bright region represents the free stream region where visualization particles are rich, while the dark grey region between this free stream and the airfoil surface corresponds to the separated flow region. The airfoil is seen as a black shadow in this image, and its lower surface cannot be seen because the light sheet is applied from the top. Please note that the reference velocity was not acquired simultaneously with the images shown in Fig. 3 in order to obtain images that are not contaminated by laser beams of the 1D-LDA. The correspondence of Fig. 1 (a) and Fig. 3 is based on Ref. 10, which performed thorough investigations of smoke flow visualization images and the reference velocity that are acquired simultaneously with each other. Ref. 10 reported that the reference velocity is large when the flow is attached to the airfoil surface while the reference velocity is small when the flow is largely separated. This relation is true for flow oscillations that occur at angles of attack $\alpha = 11 - 12°$. There was almost no phase lug between the flow condition and the reference velocity [10]. Also, the images in Fig. 3 were taken at 500 frames/sec. This means that about 250 images were taken in one period of the 2 Hz oscillation, which was enough to track the oscillation and determine the phase in the oscillation. In this way, the phase of each image shown in Fig. 3 was estimated and is shown in the caption.

In Fig. 3 (a), the flow is attached to the airfoil on the whole, although a series of small vortices observed on the airfoil surface suggest a possibility of a small separation near the leading edge. This condition approximately corresponds to $\phi \approx 0°$ in Fig. 1. This type of flowfield will be hereafter referred to as an 'attached flow.' The instant when this image was taken is defined as $t = 0$ sec. At $t = 0.1$ sec ($\phi \approx 65°$), larger vortices appear on the airfoil surface, for example, around $x/c = 0.6$ (Fig. 3 (b)). The flow near the leading edge seems to be separated from the surface at this instant. The flow over the airfoil becomes separated from the leading edge at $t = 0.2$ sec ($\phi \approx 130°$, Fig. 3 (c)). Formation of large vortices (for example, around $x/c = 0.4$) is also observed. The separated flow region expands further in height at $t = 0.3$ sec ($\phi \approx 195°$, Fig. 3 (d)). Large vortices are developing at $x/c = 0.3$, 0.6 and 1. This type of flow will be referred to as a 'separated flow.' The flowfield at $t = 0.4$ ($\phi \approx 260°$, Fig. 3 (e)) is similar to that at $t = 0.3$ sec: a large separated flow covers the entire airfoil surface. A vortex is observed around $x/c = 0.5$. At $t = 0.5$ sec ($\phi \approx 325°$, Fig. 3 (f)), a large vortex-like structure is observed near $x/c = 0.75$, and the flow near the leading edge becomes almost attached to the airfoil surface. This structure will be discussed in detail in the following section. At $t = 0.55$ sec (not shown in Fig. 3), the flow becomes attached to the airfoil surface again. In this way, the flow over the airfoil repeats switching between the attached flow and the separated flow with a period of approximately 0.5 sec (2 Hz). Please note that these images were picked out at intervals of 0.1 msec to present an overview of the oscillation. Vortices seen in the consecutive images in Fig. 3 are not associated with each other.

### 4.2 Wavelet Analysis

The wavelet analysis was applied to the reference velocity fluctuations at some angles of attack near stall to investigate their characteristics. The reference velocities at $\alpha = 11.3°$, 11.5°, 11.8° and 12° were analyzed by this technique. Ref. 10 performed the Fourier analysis on the oscillation at $\alpha = 11.5°$, where the flow oscillated almost periodically.

However, the oscillation at other angles of attack could not be analyzed by Fourier analysis, since the flow oscillations were non-periodical as was described in Ref. 10. Therefore, the wavelet analysis was utilized in this study to analyze the flow fluctuations at other angles of attack as well as at $\alpha = 11.5°$.

Figs. 4 - 7 show the result of the analysis. In each figure, figure (a) shows the reference velocity fluctuation that was analyzed by the wavelet analysis technique. Figure (b) shows the result of the wavelet analysis. In this figure, the abscissa axis represents the time $t$ sec, and the ordinate represents the frequency $f$ Hz (= $1/a$). The color contour shows the real part of the wavelet coefficient $Wf(b, a)$. Red and yellow regions indicate that a peak of the velocity wave pattern exists at the corresponding time and frequency, while blue regions show that there is a trough of the wave pattern.

Fig. 4 (a) shows the time history of the reference velocity at $\alpha = 11.3°$. As was reported in Ref. 10, this figure indicates that the flow is attached to the surface (i.e. the reference velocity is large) for most of the time and occasionally switches to a separated flow (i.e. the reference velocity is small), for instance, at $t$ = 1 sec and $t$ = 3 sec. This switching is analyzed in Fig. 4 (b). At $t$ = 1 sec and $t$ = 3 sec, there are blue regions representing the troughs in the velocity wave pattern around 1.5 Hz. This frequency corresponds to a Strauhal number of $St$ = 0.0059. This frequency is slightly lower than that observed at $\alpha = 11.5°$, which was approximately 2 Hz [10]. The amplitude of the oscillation is also smaller at this angle of attack than that observed at other angles of attack which will be discussed later on.

Fig. 5 (a) shows the reference velocity fluctuation at $\alpha = 11.5°$. This figure shows that the flow repeats the switching between the attached flow and the separated flow at about 2 Hz as has been discussed in Ref. 10. Fig. 5 (b) shows the result of the wavelet analysis on the wave pattern shown in Fig. 5 (a). Fig. 5 (b) shows that the frequency of the velocity fluctuation is about 2 Hz ($St$ = 0.008). This result well agrees with the result of the Fourier analysis performed in Ref. 10. A slight change in frequency is observed between $t$ = 1 sec - 2 sec and $t$ = 2 sec - 4 sec.

Fig. 6 (a) shows the time history of the reference velocity at $\alpha = 11.8°$. At this angle of attack, although the reference velocity shows a quasi-periodic oscillation occasionally (e.g. $t$ = 1 sec - 2.5 sec), the reference velocity stays small (i.e. the flow is largely separated) for longer time than at $\alpha = 11.5°$. This trend was also reported in Ref. 10. The result of the wavelet analysis shown in Fig. 6 (b) shows the velocity fluctuation approximately as strong as at $\alpha = 11.5°$ at $t$ = 1 sec - 3 sec. Weaker fluctuations are observed at $t$ = 3 sec - 5 sec. Both strong and weak fluctuations observed at this angle of attack have a frequency of about 2 Hz ($St$ = 0.0082).

Fig. 7 (a) shows the reference velocity at $\alpha = 12.0°$. At this angle of attack, the reference velocity stays small (i.e. the flow is largely separated) for most of the time. Small fluctuation exists, for instance, at $t$ = 3 sec - 4 sec. The waveform appears different from that at other angles of attack in that the amplitude of the fluctuation is relatively small. The result of the wavelet analysis on this wave pattern is shown in Fig. 7 (b). There are faint yellow and blue regions which represents the peak and trough of the wave pattern. The frequency of the fluctuation is around 3 Hz ($St$ = 0.012).

### 4.3 Instantaneous Flowfield Measurements

In order to investigate the flow phenomenon that causes the flow to oscillate, PIV flowfield measurements were performed. The discussions in this section focus on the flowfield at $\alpha = 11.5°$, where the oscillation occurs quasi-periodically.

The results of the PIV measurements are shown in Figs. 8 - 10 for three different phases: $\phi \approx 0°$ in Fig. 8, $\phi \approx 130°$ in Fig. 9 and $\phi \approx 300°$ in Fig. 10. In Figs. 8 - 10, figure (a) shows the smoke flow visualization image which was already presented in Fig. 3 to understand the entire flowfield on the airfoil. Figures (b) - (d) show the PIV results of $x/c$ = 0 - 0.07, and figures (e) - (g) show the results of $x/c$ = 0 - 0.07.

Figures (b) and (e) show the reference velocities. The black curves represent the reference velocity, and the red vertical bars indicate the timings of the PIV laser pulses. The timings of the PIV pulses corresponding to images shown in (d) and (g) are notated by "(d)" and "(g)" respectively. Raw images used for the PIV measurements are shown in figures (c) and (f). Figures (d) and (g) show the instantaneous velocity field measured by PIV. The velocity vectors on these images are placed too densely to see vectors in the free stream region. However, these figures are intended to show the velocity distribution in the separated flow region, which is of the greatest interest in this study. The color contours in the figures show the spanwise vorticity distribution. The spanwise vorticity $\omega$ is defined as

$$\omega = \frac{\partial V}{\partial x} - \frac{\partial U}{\partial y} \qquad (5)$$

The red and yellow contours represent the vorticity in the counterclockwise direction, and the blue contours correspond to the clockwise vorticity. In some figures, some part of the contour map is missing, especially inside shear layers and vortices. This is due to the post processing of the PIV results which includes removal of erroneous vectors. The erroneous vector removal was carried out based on the magnitude of the vectors: the vectors which exceed $3U_\infty$ in magnitude were omitted because the flow velocities are expected to be less than $3U_\infty$. Occurrence of erroneous vectors is unavoidable in the present study because PIV is weak in detecting rotational motions of visualizing particles and because the visualizing particles are scarce in the separated region [13]. The black curve near the bottom of the figure represents the airfoil surface. The PIV images are taken at a rate of 5 Hz. This is far from enough time resolution to track the 2 Hz flow oscillation. Therefore, the images presented here are selected to present the characteristic flowfield of each phase.

It should be noted that (a), (b) and (c) are the results of experiments performed separately. The correspondence of these three figures is confirmed by examining the reference velocity and estimating the approximate phase for each figure. However, due to the low sampling rate of the PIV, the phase of each figure does not exactly agree with the designated value. The phase of the flow visualization images shown in figure (a) was determined by tracking consecutive images, as was done in section 4.1.

Fig. 8 shows the flowfield which is attached to the airfoil surface ($\phi \approx 0°$). In Fig. 8 (d), a blue region, which represents a shear layer, extends along the airfoil surface slightly above the surface. The distance between the shear layer and the surface is much closer than in other images. There is a reverse flow region between the surface and the shear layer. This indicates that the flow is slightly separated from the surface. In Fig. 8 (g), the flow is moving toward the airfoil surface at around $x/c \approx 0.12$. This suggests that the flow reattaches to the surface at this point. This reattachment location approximately matches that of a short bubble observed at a lower angle of attack ($x/c \approx 0.1$ at $\alpha = 10°$ [2]). Ref.8 also discussed that a separation bubble which is similar to a short bubble at $\alpha = 10°$ seems to be formed at this phase of $\phi = 0°$.

Fig. 9 shows the instantaneous flowfield at $\phi \approx 120°$. At this phase, the flow over the airfoil becomes separated on the entire airfoil surface (Fig. 9 (a)). In Fig. 9 (d), a shear layer (blue region) moves farther away from the airfoil surface than that in Fig. 8 (d). The reverse flow region between the shear layer and the surface is fairly smooth, with no vortices observed. Other results of the PIV measurements at this location ($x/c$ = 0 - 0.07) also showed no vortex in the separated flow region around this phase. Fig. 9 (g) shows many vortices are formed downstream of $x/c$ = 0.08. An extremely large vortex about 3 % of the chord length in diameter is observed at $x/c$ = 0.11. This vortex may have caused the slight drop of the reference velocity at the instant when this image was acquired (see Fig. 9 (e)). Since the reference velocity was measured in the free stream region upstream of this vortex, this large vortex seems to affect the entire flowfield over the airfoil. The shear layer,

which was thin upstream of the $x/c$ = 0.07, spreads in the vertical direction and increase its thickness. There is still a reverse flow region on the airfoil surface, but unlike in Fig. 8 (d), there is counterclockwise vorticity distribution just above the surface.

Flowfield at about $\phi \approx 300°$ is presented in Fig. 10. In Fig. 10 (a), a large vortex-like structure is observed near $x/c$ = 0.75, and the flow near the leading edge becomes almost attached to the airfoil surface. A flow structure that may correspond to this one is observed in Fig. 10 (d) at $x/c$ = 0.06. A vortex is formed near the leading edge and is almost attached to the airfoil surface. Both of these phenomena were not observed in the PIV results at other phases. A shear layer, which extends almost linearly in other PIV results are bended toward the airfoil surface in this result. A similar phenomenon is observed in Fig. 10 (g). A vortex is observed at $x/c$ = 0.075. The free stream is introduced into the separated flow region toward the airfoil surface downstream of this vortex near $x/c$ = 0.09. The reverse flow region is moving upward, lifting the shear layer and the vortices around $x/c$ = 0.1 - 0.13. The vortex-like structure observed at $x/c$ = 0.75 in Fig. 10 (a) seems to correspond to this lifted shear layer.

### 4.4 Discussions

The results of the wavelet analysis showed that the Strauhal number of the flow fluctuation increases as the angle of attack is increased. This trend was reported in Ref. 7, which performed wind tunnel experiments of various airfoils. However, detailed natures of this trend have not yet been known. It was also observed that the frequency slightly changes with time (see Figs. 6 (b) and 7 (b)). This change in frequency with time and the change in frequency with the angle of attack may be related to each other. Instantaneous flowfield investigations together with wavelet analysis may present more understanding of these phenomena.

From results of the smoke flow visualizations and the PIV flowfield measurements, the flow oscillation is occurring as summarized below:

1) The flow is attached to the airfoil surface on the whole. There is a small separation bubble near the leading edge that resembles a short bubble formed at a lower angle of attack (Fig. 8).
2) The separation bubble increases its length, and the shear layer moves away from the airfoil surface. Series of vortices are formed near the leading edge and move downstream in the shear layer (Fig. 9).
3) When the separated region grows large, a large vortex, which bends the shear layer toward the airfoil surface, is formed near the leading edge (Fig. 10).
4) The flow reattaches to the airfoil surface and returns to an attached flow.

Differences in behaviors of the vortices are observed among these four phases. Especially, the vortex observed in Fig. 10 is worth noting. This vortex is formed closest to the leading edge than at any other phases. It bends the shear layer toward the airfoil surface and introduces the free stream into the separated flow region (Fig. 10 (d) and (g)). The flow upstream of the vortex is almost attached to the airfoil surface (Fig. 10 (a)). Therefore, this vortex may be a part of the mechanism that switches the flow from a separated condition to an attached flow. Further investigations on this vortex including PIV measurements and wavelet analysis are expected to reveal more of the flow oscillation.

It was also suggested by Ref. 7 that the low-frequency oscillation under investigation is of the same kind as the shear layer flapping. However, no evidence was found in the results of the present measurements.

It should be noted that only the flowfield in the chordwise plane on the airfoil centerline is investigated in the present study. However, the separated flow is supposed to have three-dimensional vortex structures that vary along the spanwise direction. Also, there might be effects of the tunnel walls on the flowfield, since the experiments in the present study were carried out in a 0.2 m span wind tunnel using an airfoil model of 0.2 m chord length. Therefore, investigations on three-dimensional flow

structures are needed to fully understand the flow phenomena discussed in this paper.

## 5 Conclusions

Laminar separation bubbles formed on a NACA 0012 airfoil were investigated to clarify their quasi-periodic behaviors near the onset of airfoil stall. Measurements were performed at a chord Reynolds number of $Re_c = 1.3\times10^5$.

1) Wavelet analysis was applied to the instantaneous velocity in the free stream direction at a point near the leading edge. The results indicated flow fluctuations of about 1.5 Hz - 3 Hz near the onset of stall ($\alpha$ = 11.3° - 12°). The amplitude of the fluctuation is the greatest and the fluctuation occurred quasi-periodically at $\alpha$ = 11.5°. The frequency of this fluctuation shows a tendency to increase as the airfoil angle of attack is increased within this range of $\alpha$ = 11.3° - 12°. A slight change in frequency with time was also observed at $\alpha$ = 11.5°.
2) Formation of a large vortex near the leading edge (at about $x/c$ = 0.05) was observed when the flow switches from a large separated state to an attached flow. At this chordwise location, no vortices were observed at other phases in the oscillation. This vortex develops as it moves downstream. It deforms the shear layer on the airfoil surface and introduces the free stream into the separated flow region toward the surface. The reverse flow region and the shear layer on the airfoil downstream of the vortex become lifted into the free stream region. These changes in flowfield by this vortex may be strongly related to the mechanism that generates the flow oscillation.

## Acknowledgements

The Author would like to thank Prof. K. Rinoie for his valuable advice. Support in performing the experiments by Mr. Y. Sunada is also gratefully acknowledged.

## References

[1] Tani I. Low-Speed Flows Involving Bubble Separations, *Progress in Aeronautical Sciences*, Vol. 5, pp 70-103, 1964.

[2] Hata K, Rinoie K, Takemura N and Sunada Y. Experimental Studies of Low Frequency Velocity Disturbances Observed in Short Bubble Formed on Airfoil (in Japanese). *Journal of Japan Society for Aeronautical and Space Sciences*, Vol. 50, No. 582, pp 293-300, 2002.

[3] Zaman K B M Q, McKinzie D J and Rumsey C L. A Natural Low-Frequency Oscillation of the Flow over an Airfoil Near Stalling Conditions. *Journal of Fluid Mechanics*, Vol. 202, pp 403-422, 1989.

[4] Bragg M B, Heinrich D C and Khodadoust A. Low-Frequency Flow Oscillation over Airfoils near Stall, *AIAA Journal*, Vol. 31, No. 7, pp 1341-1343, 1993.

[5] Bragg M B, Heinrich D C and Balow F A. Flow Oscillation over an Airfoil Near Stall, *AIAA Journal*, Vol. 34, No. 1, pp 199-201, 1996.

[6] Broeren A P and Bragg M B. Flowfield Measurements over an Airfoil During Natural Low-Frequency Oscillations near Stall, *AIAA Journal*, Vol. 37, No. 1, pp 130-132, 1999.

[7] Broeren A P and Bragg M B. Unsteady Stalling Characteristics of Thin Airfoils at Low Reynolds Number. *Progress in Astronautics and Aeronautics*, Vol. 195, pp 191-213, 2001.

[8] Rinoie K and Takemura N. Oscillating Behaviour of Laminar Separation Bubble Formed on an Airfoil Near Stall, *Aeronautical Journal*, Vol. 108, No. 1081, pp 153-163, 2004.

[9] Takemura N, Rinoie K and Sunada Y. Low Frequency Oscillation of Laminar Separation Bubble Near Stall –Discussion on Turbulent Energy Production– (in Japanese). *Journal of Japan Society for Aeronautical and Space Sciences*, Vol. 52, No. 602, pp 114-120, 2004.

[10] Tanaka H, Rinoie K and Sunada Y. Visualization of the Laminar Separation Bubble Oscillating at Low Frequency on an Airfoil near Stall (in Japanese). *Proc the 35th Fluid Dynamics Conference*, Kyoto, Japan, paper number 1D2, pp 183-186, 2003.

[11] Yamada M. Wavelets and Data Analysis. *Proc the 28th Fluid Dynamics Conference*, Toyama, Japan, paper number S-2, pp. S7-S15, 1996.

[12] Li H. Identification of Coherent Structure in Turbulent Shear Flow With Wavelet Correlation Analysis. *ASME Journal of Fluids Engineering*, Vol. 120, No. 4, pp 778-785, 1998

[13] The Visualization Society of Japan, ed. *Handbook of Particle Image Velocimetry* (in Japanese). 1st edition, Morikita Shuppan, 2002.

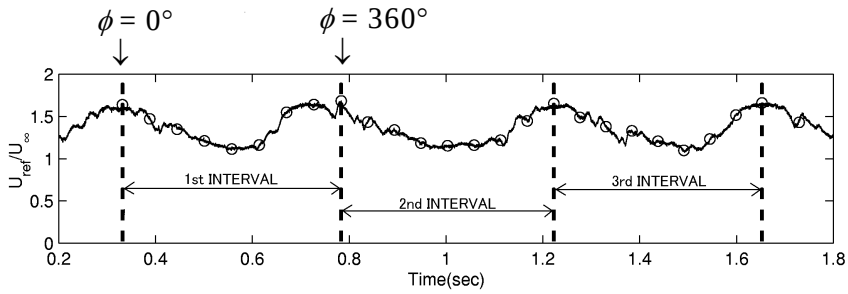


(a) Time History of the Reference Velocity

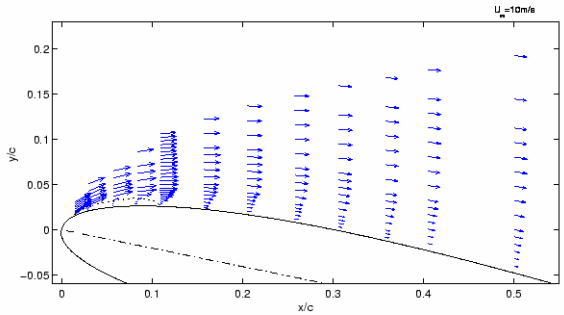

ϕ = 0°

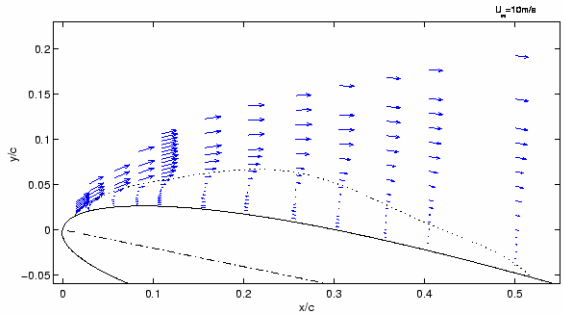

ϕ = 90°

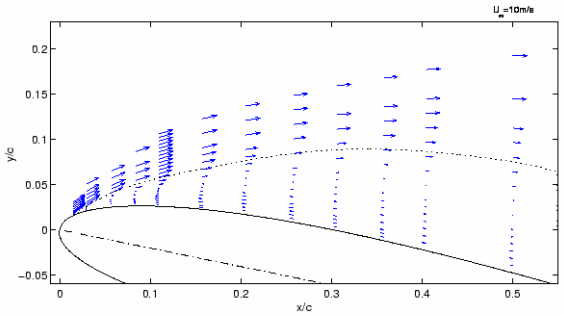

ϕ = 180°

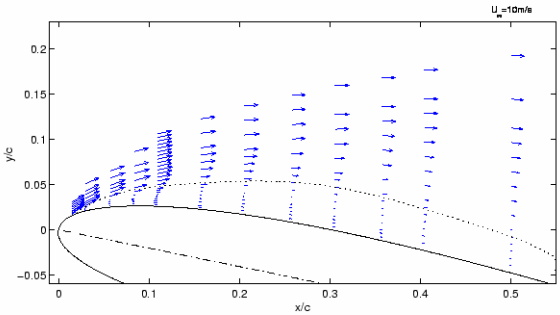

ϕ =270°

(b) Phase Averaged Velocity Distributions (The dotted line represents the dividing streamline)

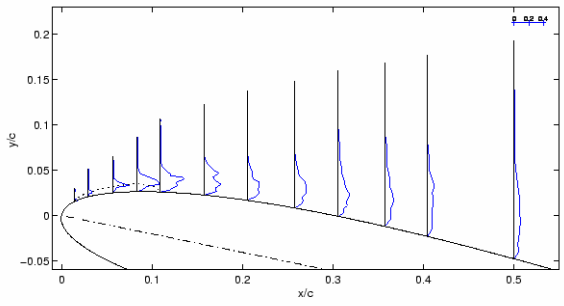

ϕ = 0°

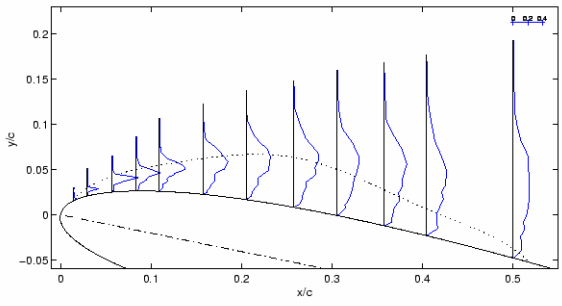

ϕ = 90°

(c) Phase Averaged Normal Turbulent Stress $\overline{u^2}$ Dttistributions

Fig. 1. Phase Averaged Measurements of the Low-Frequency Oscillation (α = 11.5°) [8]

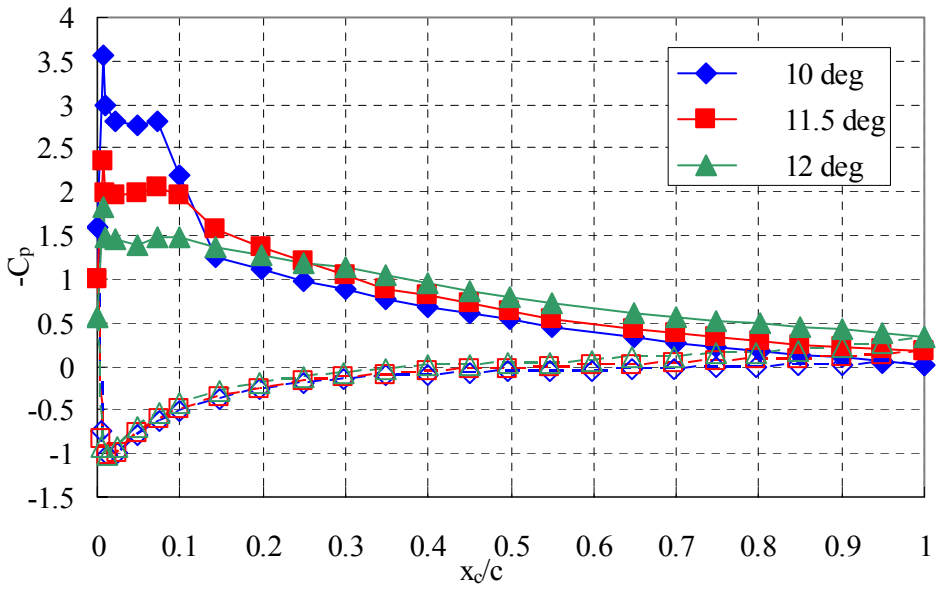


Fig. 2. Surface Pressure Distributions [2]

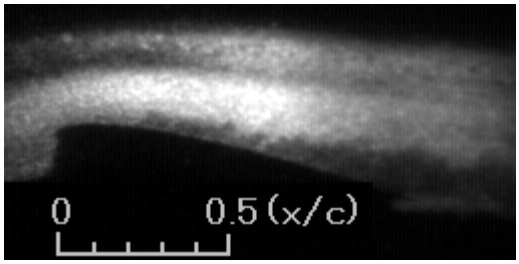


(a) $t$ = 0 sec ($\phi \approx 0°$)

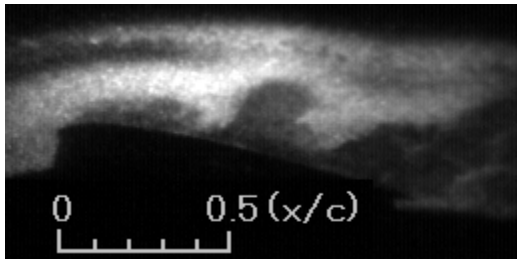


(b) $t$ = 0.1 sec ($\phi \approx 65°$)

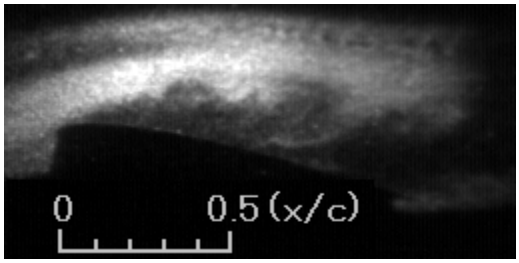


(c) $t$ = 0.2 sec ($\phi \approx 130°$)

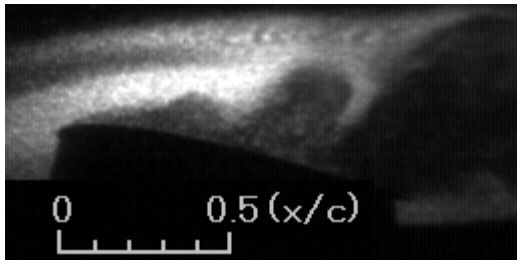


(d) $t$ = 0.3 sec ($\phi \approx 195°$)

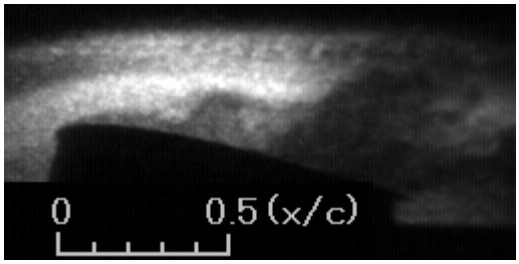


(e) $t$ = 0.4 sec ($\phi \approx 260°$)

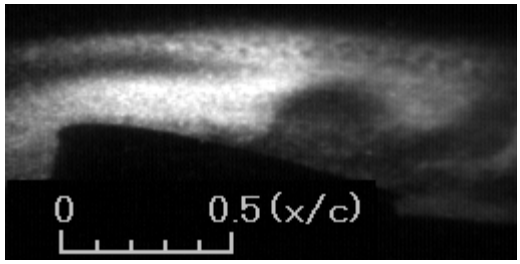


(f) $t$ = 0.5 sec ($\phi \approx 325°$)

Fig. 3. Smoke Flow Visualization at $\alpha$ = 11.5°
($\phi$ is the estimated phase angle in this figure.)

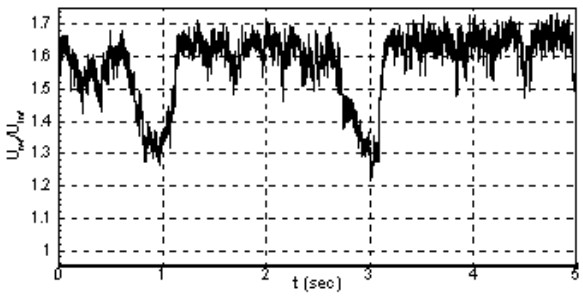


(a) Reference Velocity

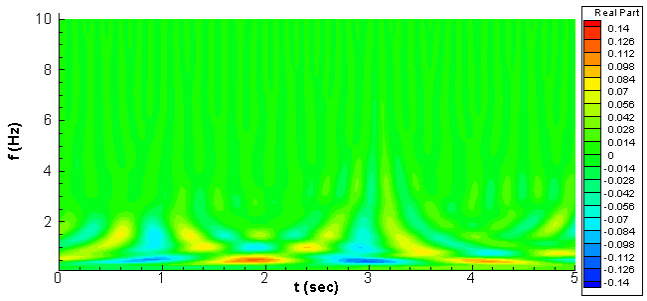


(b) Real Part of $Wf(b, a)$

Fig. 4. Results of the Wavelet Analysis at $\alpha = 11.3°$

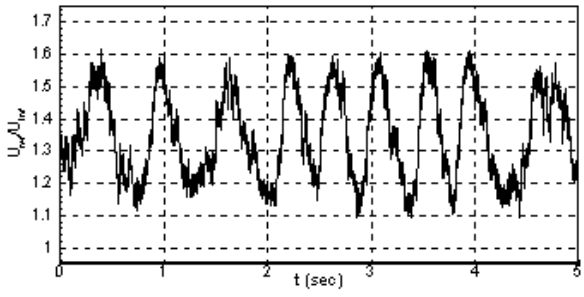


(a) Reference Velocity

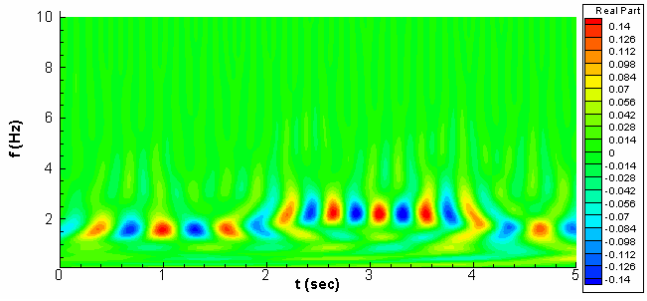


(b) Real Part of $Wf(b, a)$

Fig. 5. Results of the Wavelet Analysis at $\alpha = 11.5°$

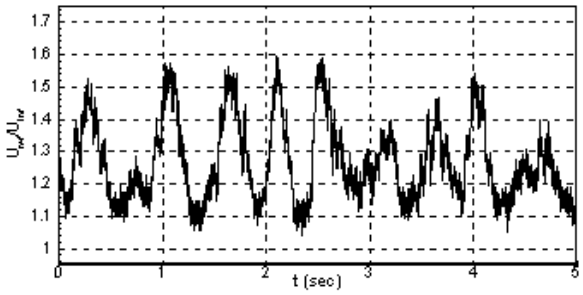


(a) Reference Velocity

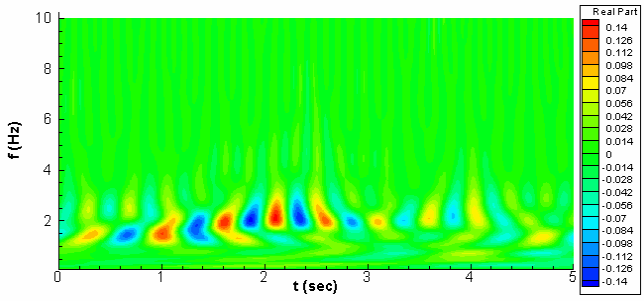


(b) Real Part of $Wf(b, a)$

Fig. 6. Results of the Wavelet Analysis at $\alpha = 11.8°$

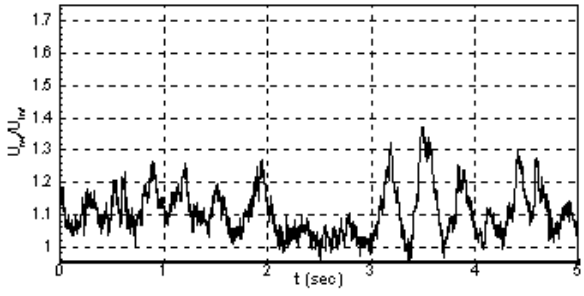


a) Reference Velocity

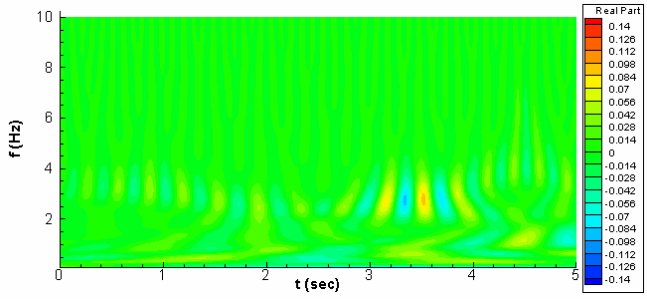


(b) Real Part of $Wf(b, a)$

Fig. 7. Results of the Wavelet Analysis at $\alpha = 12°$

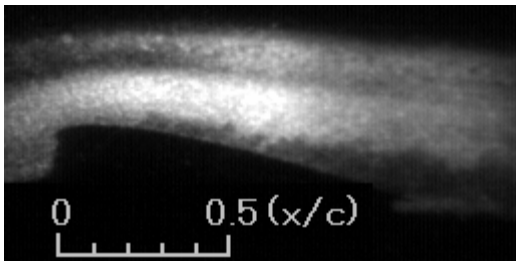


(a) Smoke Flow Visualization ($t$ = 0 sec)

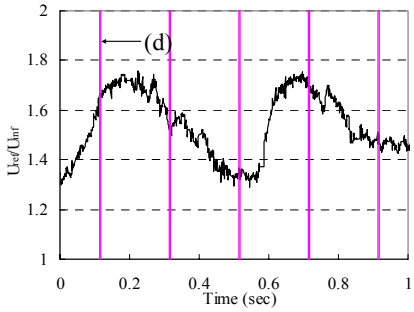


(b) Reference Velocity and PIV pulse

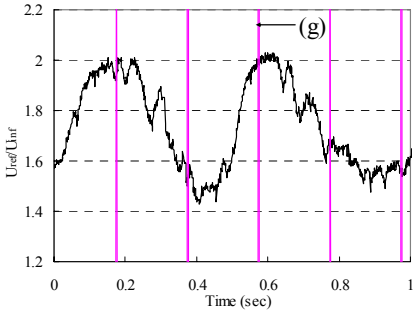


(e) Reference Velocity and PIV pulse

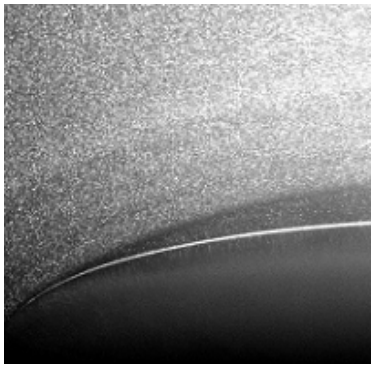

(c) Raw PIV Image ($x/c$ = 0 - 0.07)

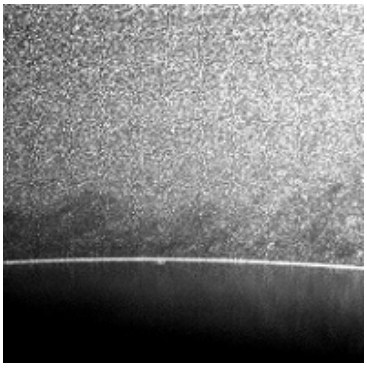

(f) Raw PIV Image ($x/c$ = 0.07 - 0.14)

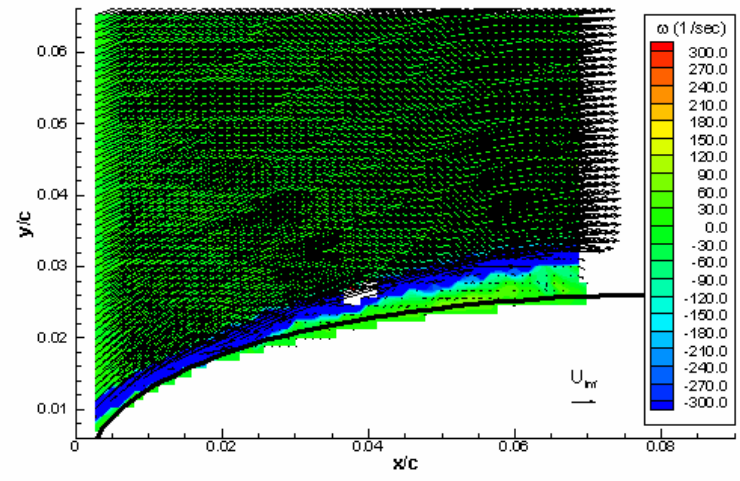


(d) Velocity Field Distribution ($x/c$ = 0 - 0.07)

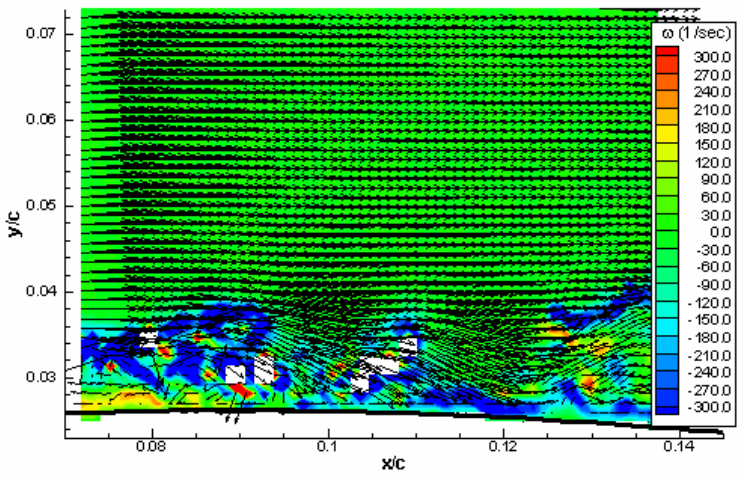


(g) Velocity Field Distribution ($x/c$ = 0.07 - 0.14)

Fig. 8. Instantaneous Flowfield ($\phi \approx 0°$, $\alpha = 11.5°$)

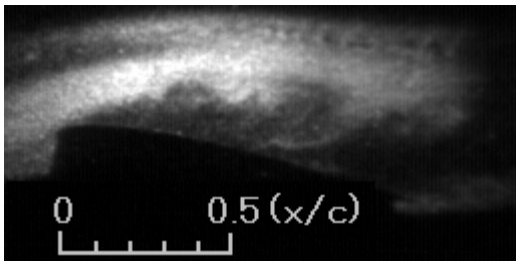


(a) Smoke Flow Visualization ($t$ = 0.2 sec)

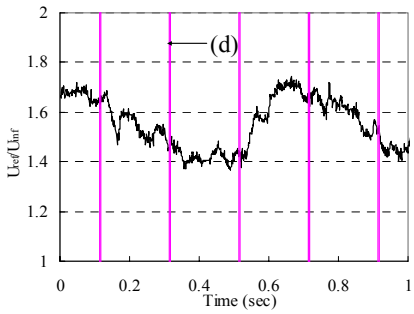


(b) Reference Velocity and PIV pulse

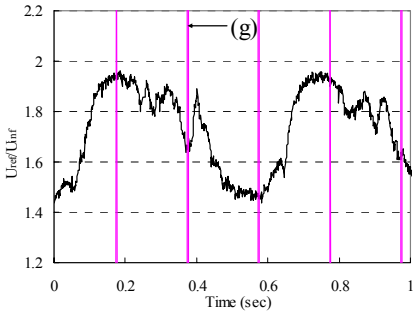


(e) Reference Velocity and PIV pulse

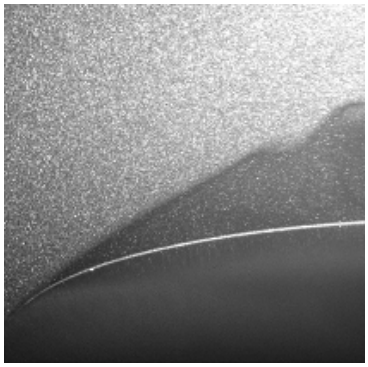

(c) Raw PIV Image ($x/c$ = 0 - 0.07)

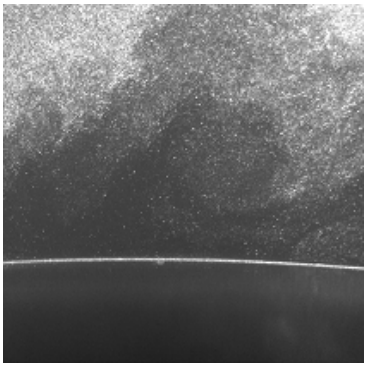

(f) Raw PIV Image ($x/c$ = 0.07 - 0.14)

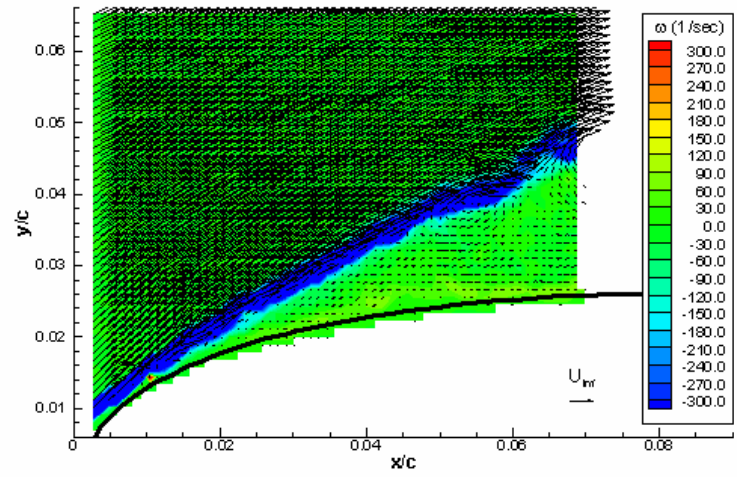


(d) Velocity Field Distribution ($x/c$ = 0 - 0.07)

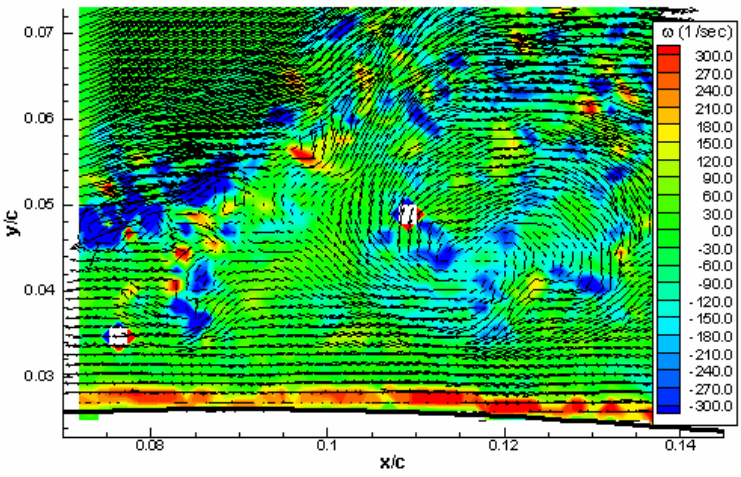


(g) Velocity Field Distribution ($x/c$ = 0.07 - 0.14)

Fig. 9. Instantaneous Flowfield ($\phi \approx 120°$, $\alpha = 11.5°$)

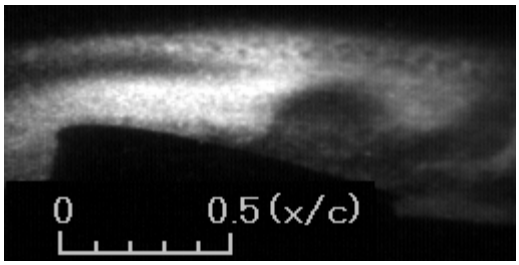


(a) Smoke Flow Visualization ($t$ = 0.5 sec)

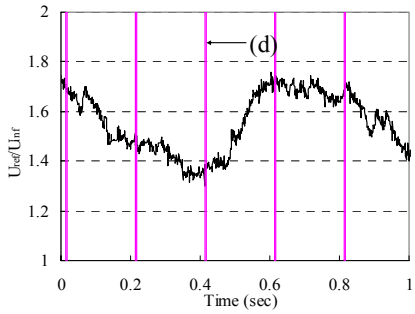


(b) Reference Velocity and PIV pulse

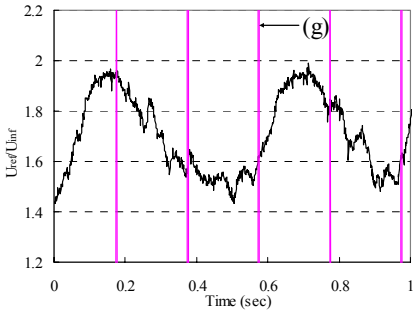


(e) Reference Velocity and PIV pulse

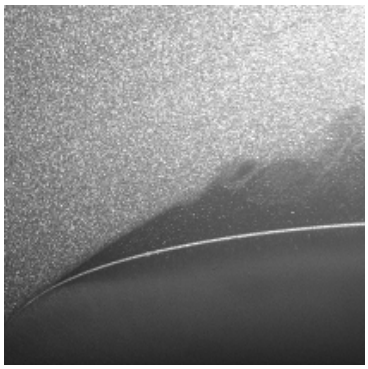

(c) Raw PIV Image ($x/c$ = 0 - 0.07)

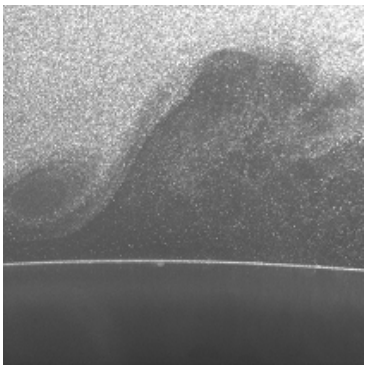

(f) Raw PIV Image ($x/c$ = 0.07 - 0.14)

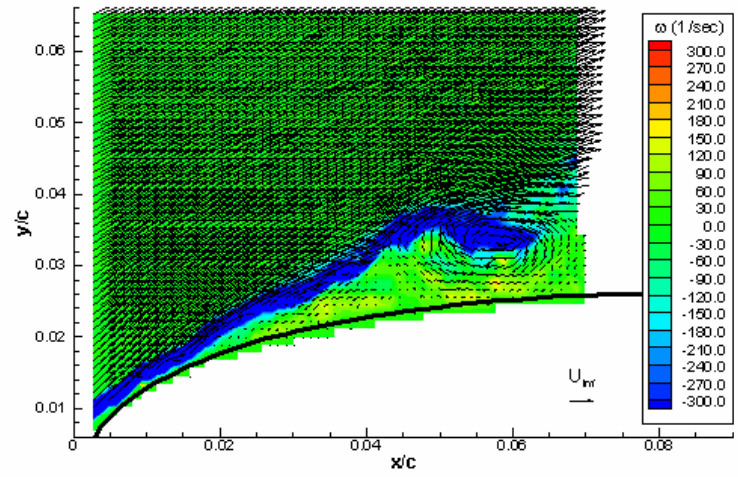


(d) Velocity Field Distribution ($x/c$ = 0 - 0.07)

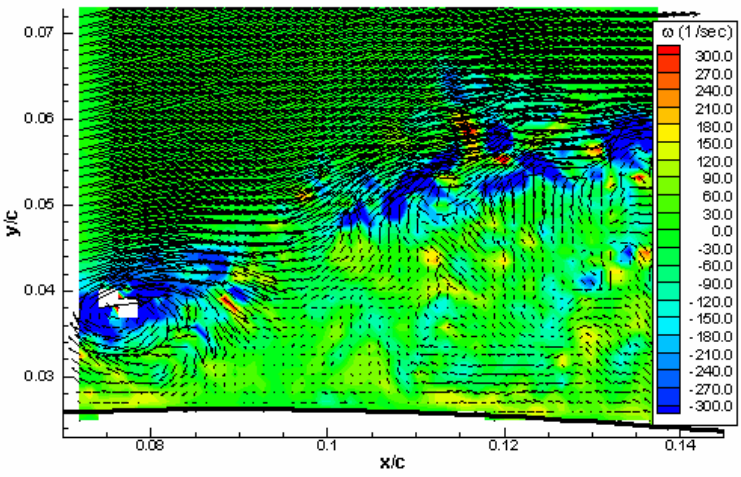


(g) Velocity Field Distribution ($x/c$ = 0.07 - 0.14)

Fig. 10. Instantaneous Flowfield ($\phi \approx 300°$, $\alpha = 11.5°$)